Analysis of co-current hydraircooling of food products in bulk

K. V. Narasimha Rao, G. S. V. L. Narasimham and M. V. Krishna Murthy
Department of Mechanical Engineering, Indian Institute of Science, Bangalore, India

A mathematical model is developed to describe the hydraircooling process when the water and air are flowing in the same direction. The governing equations for the simultaneous heat and mass transfer are solved using finite-difference numerical methods. The half cooling time of the food products is correlated as a function of the dimensionless process parameters. It is observed that a process time of approximately double the half cooling time will result in the food products attaining almost a steady state. The process times of the bulk hydraircooling process and the bulk air precooling process are compared.

Keywords: precooling technique; hydraircooling; half cooling time

Introduction

The importance of heat and mass transfer in food processing and preservation technology has been reviewed by Krishna Murthy and Badarinarayana (1978) and Gaffney et al. (1985). The aim of all food processing and preservation operations is to retard metabolic activity and growth of microorganisms so that the product can be preserved for a longer time. All food preservation methods use a *cold chain* that involves precooling the food products to the storage conditions, or precooling and freezing the food products for storage and distribution. By definition, *precooling* refers to rapid removal of field heat in the food products prior to shipment or storage. This takes place soon after the harvest or gathering. Various types of precooling techniques like air cooling, hydrocooling, and hydraircooling are discussed in detail in ASHRAE Guide and Data Book (1971) and by Hall (1974).

Hydraircooling is an effective method of precooling food products for which moisture loss is not desirable. It has the advantages of both air cooling and hydrocooling. When cold air is passed over food products that are continuously wetted by a thin film of water, there will be more effective cooling without much dehydration of the product. An analysis of such a process for an isolated, single product has been presented by Abdul Majeed (1981). The present article presents a theoretical analysis of the hydraircooling of spherical food products cooled in bulk with water and air flowing in the same direction. The governing equations for the product, film, interstitial water spray, and moist air are solved using finite-difference methods. Time–temperature histories are obtained in terms of dimensionless parameters covering a wide range of the product properties and processing conditions encountered in food precooling practice.

Address reprint requests to Professor Krishna Murthy at Department of Mechanical Engineering, Indian Institute of Science, Bangalore 560012, India.

Received 30 July 1991; accepted 27 January 1992

Theoretical analysis

Description of the physical model

The physical model consists of a number of layers of spherical food products packed in the form of a rectangular parallelepiped (Figure 1). The geometry of the food product is chosen to be spherical because a large variety of fruits and vegetables can be satisfactorily approximated by this shape. Chilled water is sprayed from the top onto the products so as to produce a thin film of water over each product (Figure 2). The air is also inducted from the top of the package in the same direction as that of the water with the help of an air blower. The food products are packed in horizontal layers, one below the other in an in-line arrangement in the vertical direction. The flowing water film envelops the food product and experiences a certain amount of evaporation or condensation depending on the direction of driving potential for mass transfer. When the film approaches the bottom of the product, the water gravitates onto the next food product directly below. This gives rise to the formation of a water film on the succeeding product. Chilled water not intercepted by the products flows through the interstitial space of the package. It is necessary to leave a small air gap between the product layers in the vertical direction to facilitate easy loading and unloading in practical situations. If the radius of the product is denoted by R and the height of the air gap by B, the overall height of the package, H, containing L layers will be $L \cdot 2R + (L - 1)B$, as shown in Figure 1.

A spherical coordinate system is employed for the food product, with the radius r measured from the center of the product, while a Cartesian coordinate system is used with the z-coordinate measured from the top of the package for the interstitial water spray and the moist air. Thus, $z = H$ corresponds to the bottom of the package, which is the exit for both air and water.

Initially, all the food products in the package are assumed to be at a uniform temperature T_{po}. The package is then exposed to a chilled water spray at a temperature of T_{fe} and to cold unsaturated air at a temperature of T_{mae}. The products are cooled by the combined action of chilled water and air. The conditions of entering water and air are maintained constant throughout.

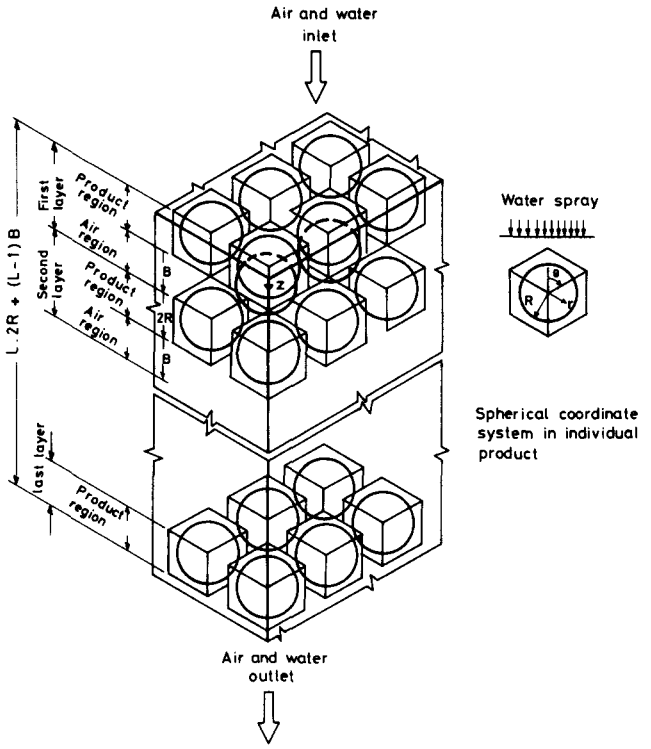

Figure 1 The physical model and coordinate system for bulk hydraircooling of food products

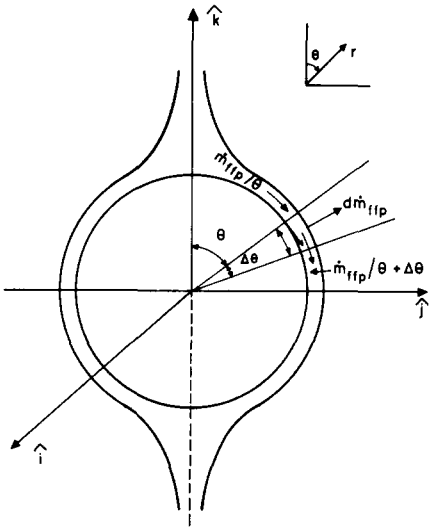

Figure 2 Physical model

Mathematical formulation

The governing equations are written separately for the product, the water film over the product, the interstitial water spray, and the moist air.

Notation

a	Thermal diffusivity ($m^2 \cdot s^{-1}$)
A	Area (m^2)
A_0, A_1, A_2	Coefficients defined in Equation 26
B_0, B_1, B_2	Coefficients defined in Equation 45
C_0, C_1, C_2	Coefficients defined in Equation 47
C_p	Specific heat ($kJ \cdot kg^{-1} \cdot K^{-1}$)
d	Diameter (m)
D	Binary diffusion coefficient of water vapor in dry air ($m^2 \cdot s^{-1}$)
$D_1 - D_4$	Coefficients defined in Equation 60
Fo	Fourier number (dimensionless)
Fr	Froude number (dimensionless)
g	Acceleration due to gravity ($m^2 \cdot s^{-1}$)
h_v	Enthalpy of water vapor ($kJ \cdot kg^{-1}$)
Δh_v	Latent heat of vaporization ($kJ \cdot kg^{-1}$)
H	Height of the package measured from the top (m)
Ja	Jakob number (dimensionless)
L	Number of layers
$\dot{m}$	Mass flow rate ($kg \cdot s^{-1}$)
Nu	Nusselt number (dimensionless)
Pr	Prandtl number (dimensionless)
q_{int}	Heat of respiration in the food product ($W \cdot m^{-3}$)
r	Radial coordinate
R	Radius of the spherical food product (m)
Re	Reynolds number (dimensionless)
Sc	Schmidt number (dimensionless)
Sh	Sherwood number (dimensionless)
t	Time (s)
T	Temperature (°C)
v_θ	Tangential velocity in the film ($m \cdot s^{-1}$)
w	Average velocity ($m \cdot s^{-1}$)
W	Humidity ratio (kg per kg of dry air)
z	Coordinate along the height of the package

Greek symbols

α_h	Heat transfer coefficient ($W \cdot m^{-2} \cdot K^{-1}$)
α_m	Mass transfer coefficient ($kg \cdot m^{-2} \cdot s^{-1}$)
δ	Film thickness (m)
λ	Thermal conductivity ($W \cdot m^{-1} \cdot K^{-1}$)
μ	Dynamic viscosity ($N \cdot s \cdot m^{-2}$)
ν	Kinematic viscosity ($m^2 \cdot s^{-1}$)
ψ	Void fraction (dimensionless)
θ	Angular coordinate
ρ	Density ($kg \cdot m^{-3}$)
$\tau_{1/2}$	Half cooling time (dimensionless)

Subscripts

e	Entry
f	Water film
fbm	Water bulk mean
fi	Interstitial water spray
o	Initial
ma	Moist air
p	Product
s	Saturated, superficial
u	Per unit volume of the package
wb	Wet bulb
wd	Water droplet

Superscripts

*, **	Dimensionless quantity

Product. Assuming symmetry about the vertical axis of the product (i.e., neglecting the variation of temperature in the azimuthal direction), the transient conduction equation for a homogeneous, isotropic product with temperature-independent thermal properties, negligible moisture-concentration gradients, and negligible moisture evaporation can be written as

$$\frac{\partial^2 T_p}{\partial r^2} + \frac{2}{r}\frac{\partial T_p}{\partial r} + \frac{\cot\theta}{r^2}\frac{\partial T_p}{\partial \theta} + \frac{1}{r^2}\frac{\partial^2 T_p}{\partial \theta^2} + \frac{q_{int}}{\lambda_p} = \frac{1}{a_p}\frac{\partial T_p}{\partial t} \tag{1}$$

where q_{int} is the heat of respiration within the food product and is taken constant at $52\ W \cdot m^{-3}$ for fruits and vegetables such as apples, cabbage, lettuce, etc. (ASHRAE Handbook of Fundamentals 1989).

Liquid film. The coordinate system for the liquid film is shown in Figure 2. In view of the thinness of the film [$\mu_f \rho_f \gg \mu_{ma} \rho_{ma}$], the transverse pressure gradient is neglected. Also, since the impressed pressure is taken as constant, the streamwise pressure gradient becomes zero. The governing equation for the momentum in the liquid film with quasi-steady approximation is written as follows:

Momentum equation

$$\mu_f \frac{d^2 v_\theta}{dr^2} + \rho_f g \sin\theta = 0 \tag{2}$$

The above equation is written under the assumption that the viscous forces balance the gravitational forces, and hence the acceleration terms are negligible.

Energy equation

$$\frac{\partial T_f}{\partial t} + \frac{v_\theta}{R}\frac{\partial T_f}{\partial \theta} = a_f\left\{\frac{\partial^2 T_f}{\partial r^2} + \frac{1}{R^2}\frac{\partial^2 T_f}{\partial \theta^2}\right\} \tag{3}$$

The rate of evaporation or condensation at the film surface is given by the following mass conservation equation:

$$\frac{d\dot{m}_{ffp}}{d\theta} = \alpha_{mf} 2\pi R^2 \sin\theta (W_{sf} - W_{ma}) \tag{4}$$

Water spray

Mass conservation

$$\frac{d\dot{m}_{fi}}{dz} = -\alpha_{mwd} A_c A_{wdu} (W_{swd} - W_{ma}) \tag{5}$$

Here A_{wdu} is the area of water droplets available per unit volume of the package. The determination of this quantity requires the diameter of the water droplet and the number of water droplets contained in unit volume of the package. Both the water-droplet diameter and its velocity depend on parameters such as the type of pressure nozzle, the pressure drop across the nozzle, etc. In the present investigation, an average droplet diameter of 0.85 mm and an average droplet velocity of $10\ m \cdot s^{-1}$ are used (Ranz and Marshall 1952). The value of A_{wdu} can then be calculated if the mass flow rate of water through the interstices is known. However, as will be seen later, these assumptions have very little influence on the final results, and the interstitial water spray is found to have a negligible effect on the bulk hydraircooling process.

Energy equation

$$\frac{\partial T_{wd}}{\partial t} + w_{wds}\frac{\partial T_{wd}}{\partial z} = \frac{w_{wds}}{\dot{m}_{fi}} T_{wd}[\alpha_{mwd} A_c A_{wdu}(W_{swd} - W_{ma})] - \frac{w_{wds}}{\dot{m}_{fi} c_{pf}}[\alpha_{mwd} A_c A_{wdu}(W_{swd} - W_{ma}) h_v + \alpha_{hwd} A_c A_{wdu}(T_{swd} - T_{ma})] \tag{6}$$

Moist air. In formulating the moist-air governing equations, it is assumed that the temperature and humidity ratio vary only in the z-direction.

Energy equation. The equation for the conservation of energy of the moist air is written as follows:

$$\rho_{ma} C_{pma}\left(\psi\frac{\partial T_{ma}}{\partial t} + w_s\frac{\partial T_{ma}}{\partial z}\right) = \psi\lambda_{ma}\frac{\partial^2 T_{ma}}{\partial z^2} + \alpha_{hf} A_{fu}(T_{sf} - T_{ma}) + \alpha_{hwd} A_{wdu}(T_{swd} - T_{ma}) \tag{7}$$

where ψ is the void fraction, which is defined as the volume of the voids to that of the package in any product layer. ψ assumes a value of 1.0 in the air region between the product layers.

Conservation of species. The equation for the conservation of water vapor in the moist air is written as follows:

$$\rho_{ma}\left(\psi\frac{\partial W_{ma}}{\partial t} + w_s\frac{\partial W_{ma}}{\partial z}\right) = \psi\rho_{ma} D\frac{\partial^2 W_{ma}}{\partial z^2} + \alpha_{mf} A_{fu}(W_{sf} - W_{ma}) + \alpha_{mwd} A_{wdu}(W_{swd} - W_{ma}) \tag{8}$$

Initial and boundary conditions

Product and film. The initial uniform temperature of the product is expressed as follows:

$$T_p = T_{po} \quad \text{at } t \leqslant 0 \text{ for } 0 \leqslant r \leqslant R \text{ and } 0 \leqslant \theta \leqslant \pi \tag{9}$$

$$T_p \text{ remains finite as } r \text{ tends to } 0 \tag{10}$$

The continuity of heat flux and no temperature jump at the product-film interface gives

$$-\lambda_p\frac{\partial T_p}{\partial r} = -\lambda_f\frac{\partial T_f}{\partial r}, \text{ and } T_p = T_f = T_{if} \text{ at } r = R \text{ for } 0 < \theta < \pi \tag{11}$$

where T_{if} is the product–film interface temperature.

Symmetry of the temperature distribution about the vertical axis yields

$$\frac{\partial T_p}{\partial \theta} = 0 \text{ at } t > 0 \text{ for } 0 < r < R \text{ and at } \theta = 0 \text{ and } \theta = \pi \tag{12}$$

The boundary conditions for the film momentum equation (Equation 2) are

$$v_\theta = 0 \text{ at } r = R \tag{13}$$

$$\frac{dv_\theta}{dr} = 0 \text{ at } r = R + \delta \tag{14}$$

The assumption of initially uniform temperature of the water

film results in

$$T_f = T_{f0} \text{ at } t \leqslant 0, \text{ for } R \leqslant r \leqslant R + \delta \text{ and } 0 \leqslant \theta \leqslant \pi \quad (15)$$

Equation 11 serves as a common boundary condition to the product and film regions.

At the surface of the liquid film, which is in contact with the air, the energy transfer takes place due to the combined effect of heat and mass transfer. The temperature difference between the film surface and the adjacent air acts as the driving force for the sensible heat transfer, whereas the humidity ratio difference causes evaporation of water at the film surface, resulting in the transfer of latent heat. This boundary condition is written in terms of the sensible and latent heat transfers as follows:

$$-\lambda_f \frac{\partial T_f}{\partial r} = \alpha_{hf}(T_{sf} - T_{ma}) + \alpha_{mf}(W_{sf} - W_{ma})\Delta h_v$$

$$\text{at } t > 0 \text{ and } r = R + \delta, \text{ for } 0 \leqslant \theta \leqslant \pi \quad (16)$$

A continuous supply of spray water at T_{fe} is assumed to be available for the top layer to maintain a film of flowing water. This gives the following condition:

$$T_f = T_{fe} \text{ (first layer) or } T_{fbm} \text{ (subsequent layers)}$$

$$\text{at } t > 0 \text{ for } R < r < R + \delta \text{ and at } \theta = 0 \quad (17)$$

Here T_{fbm} represents the bulk mean temperature of the fluid collected at the bottom of the preceding food product. The value of T_{fbm} at any θ-location is calculated from the following expression:

$$\dot{m}_{ffp}|_\theta C_{pf} T_{fbm}|_\theta = \int_0^\delta \rho_f v_\theta 2\pi r \sin\theta C_{pf} T_f dr \quad (18)$$

The outflow boundary condition on temperature for the film is written as

$$\frac{\partial T_f}{\partial \theta} = 0 \quad \text{at } \theta = \pi \text{ for } R < r < R + \delta \quad (19)$$

Water spray

$$\dot{m}_{fi} = \dot{m}_{fie} = \dot{m}_{fe} - \dot{m}_{ffe} \quad \text{at } z = 0 \quad (20)$$

$$\dot{m}^*_{fi} = \dot{m}_{fi}/\dot{m}_{fe}; \quad \dot{m}^*_{ffe} = \dot{m}_{ffe}/\dot{m}_{fe}; \quad \dot{m}^*_{fie} = \dot{m}_{fie}/\dot{m}_{fe};$$

$$Pr_f = \nu_f/a_f; \quad Pr_{ma} = \nu_{ma}/a_{ma}; \quad R_m = \dot{m}_{ffpe}/\dot{m}_{fe};$$

Moist air

$$T_{ma} = T_{mao} \text{ and } W_{ma} = W_{mao} \quad \text{at } t = 0 \text{ for } 0 \leqslant z \leqslant H \quad (23)$$

$$T_{ma} = T_{mae} \text{ and } W_{ma} = W_{mae} \quad \text{at } t > 0 \text{ and at } z = 0 \quad (24)$$

$$\frac{\partial T_{ma}}{\partial z} = 0, \text{ and } \frac{\partial W_{ma}}{\partial z} = 0 \quad \text{at } z = H \quad (25)$$

The humidity ratio of saturated air can be expressed as a second-degree polynomial in terms of its temperature as follows:

$$W_s = A_0 + A_1 T_s + A_2 T_s^2 \quad (26)$$

where the coefficients A_0, A_1, and A_2 are constants shown below for a temperature range of 0–25°C.

$$A_0 = 3.879 \times 10^{-3} \text{ (dimensionless)}$$

$$A_1 = 2.173 \times 10^{-4} \ (°C^{-1}) \quad (27)$$

$$A_2 = 1.605 \times 10^{-5} \ (°C^{-2})$$

The wet-bulb temperature of the air at any point is found using the following psychrometric relation (ASHRAE Handbook of Fundamentals 1989):

$$W_{ma} = \frac{(2501 - 2.381T_{wb})W_s - (T_{ma} - T_{wb})}{2501 + 1.805T_{ma} - 4.186T_{wb}} \quad (28)$$

Nondimensionalization

To obtain the solution in a generalized form so that it is applicable to a wide variety of products and processing conditions, the following nondimensionalized variables are defined:

$$T^* = \frac{T - T_{wbe}}{T_{po} - T_{wbe}}; \quad r^* = r/R; \quad z^* = z/R; \quad H^* = H/R;$$

$$y_f^* = y_f/R, \text{ where } y_f = r - R; \quad \delta^* = \delta/R; \quad Fo = a_p t/R^2;$$

$$\lambda^* = \lambda_p/\lambda_f; \quad \lambda^{**} = \lambda_{ma}/\lambda_f; \quad a^* = a_p/a_f; \quad a^{**} = a_{ma}/a_f;$$

$$\nu^{**} = \nu_{ma}/\nu_f; \quad \rho^{**} = \rho_{ma}/\rho_f; \quad C_p^{**} = C_{pma}/C_{pf}; \quad d^*_{wd} = d_{wd}/R;$$

$$v^*_\theta = v_\theta/(\dot{m}_{ffpe}/\rho_f \nu_f R^2); \quad Re_f = \dot{m}_{ffpe}/\rho_f \nu_f R; \quad A_c^* = A_c/R^2;$$

$$Fr_f = (\dot{m}_{ffpe}/\rho_f R^2)/(gR)^{0.5}; \quad A^*_{fu} = A_{fu}R; \quad A^*_{wdu} = A_{wdu}R;$$

$$Nu_f = \alpha_{hf}2R/\lambda_{ma}; \quad Sh_f = \alpha_{mf}2R/\rho_{ma}D; \quad Re_p = w_s 2R/\nu_{ma};$$

$$Re_{wd} = w_{wds}d_{wd}/\nu_{ma}; \quad Re_{mwd} = (w_{wds} - w_s)d_{wd}/\nu_{ma};$$

$$Sc_{ma} = \nu/D; \quad Nu_{wd} = \alpha_{hwd}d_{wd}/\lambda_{ma}; \quad Sh_{wd} = \alpha_{mwd}d_{wd}/\rho_{ma}D;$$

$$\dot{m}^*_{fi} = \dot{m}_{fi}/\dot{m}_{fe}; \quad \dot{m}^*_{ffe} = \dot{m}_{ffe}/\dot{m}_{fe}; \quad \dot{m}^*_{fie} = \dot{m}_{fie}/\dot{m}_{fe};$$

$$Pr_f = \nu_f/a_f; \quad Pr_{ma} = \nu_{ma}/a_{ma}; \quad R_m = \dot{m}_{ffpe}/\dot{m}_{fe};$$

$$\dot{m}^*_{ma} = \dot{m}_{ma}/\dot{m}_{fe}; \quad Ja = C_{pf}\Delta T/\Delta h_v, \quad \Delta T = T_{po} - T_{wbe};$$

$$q^*_{int} = [q_{int}R^2/\lambda_p \Delta T]; \quad R_T = T_{wbe}/\Delta T \quad (29)$$

The governing equations are now rewritten in terms of the above nondimensionalized variables.

Dimensionless governing equations

Product

$$\frac{\partial T_p^*}{\partial Fo} = \frac{\partial^2 T_p^*}{\partial r^{*2}} + \frac{2}{r^*}\frac{\partial T_p^*}{\partial r^*} + \frac{\cot\theta}{r^{*2}}\frac{\partial T_p^*}{\partial \theta} + \frac{1}{r^{*2}}\frac{\partial T_p^{*2}}{\partial \theta^2} + q^*_{int} \quad (30)$$

Liquid film

Momentum equation

$$\frac{d^2 v^*_\theta}{dy_f^{*2}} = -\frac{Re_f}{Fr_f^2}\sin\theta \quad (31)$$

Energy equation

$$\frac{\partial T_f^*}{\partial Fo} + \frac{v^*_\theta Re_f Pr_f}{a^*}\frac{\partial T_f^*}{\partial \theta} = \frac{1}{a^*}\left[\frac{1}{\delta^{*2}}\frac{\partial^2 T_f^*}{\partial y_f^{*2}} + \frac{\partial^2 T_f^*}{\partial \theta^2}\right] \quad (32)$$

Mass conservation

$$\frac{d\dot{m}^*_{ffp}}{d\theta} = \frac{Sh_f}{2Re_f Sc_{ma}}\nu^{**}\rho^{**}2\pi\sin\theta(W_{sf} - W_{ma}) \quad (33)$$

Water spray

Mass conservation equation

$$\frac{d\dot{m}^*_{fi}}{dz^*} = -\frac{Sh_{wd}\rho^{**}\nu^{**}A^*_{wdu}A^*_c R_m}{Re_f Sc_{ma} d^*_{wd}}(W_{swd} - W_{ma}) \quad (34)$$

Energy equation

$$\frac{\partial T^*_{wd}}{\partial Fo} + \frac{Re_{wd} v^{**} Pr_f}{a^* d^*_{wd}} \frac{\partial T^*_{wd}}{\partial z^*} = \frac{Re_{wd} Sh_{wd} \rho^{**} v^{**2} A^*_{wdu} A^*_c Pr_f R_m}{Re_f Sc_{ma} d^{*2}_{wd} a^* \dot{m}^*_{fi}} (T^*_{wd} + R_T)(W_{swd} - W_{ma}) - \frac{Re_{wd} Nu_{wd} \lambda^{**} v^{**} A^*_{wdu} A^*_c R_m}{Re_f d^{*2}_{wd} a^* \dot{m}^*_{fi}} (T^*_{swd} - T^*_{ma}) - \frac{Re_{wd} Sh_{wd} \rho^{**} v^{**2} A^*_{wdu} A^*_c Pr_f R_m (1 + Ja)}{Ja\, Re_f Sc_{ma} d^{*2}_{wd} a^* \dot{m}^*_{fi}} (W_{swd} - W_{ma}) \quad (35)$$

Moist air

Energy equation

$$\psi \frac{\partial T^*_{ma}}{\partial Fo} + \frac{\dot{m}^*_{ma} Re_f Pr_f}{\rho^{**} A^*_c a^* R_m} \frac{\partial T^*_{ma}}{\partial z^*} = \psi \frac{a^{**}}{a^*} \frac{\partial^2 T^*_{ma}}{\partial z^{*2}} + \frac{Nu_f a^{**} A^*_{fu}}{2a^*} (T^*_{sf} - T^*_{ma}) + \frac{Nu_{wd} a^{**} A^*_{wdu}}{d^*_{wd} a^*} (T^*_{swd} - T^*_{ma}) \quad (36)$$

Conservation of species

$$\psi \frac{\partial W_{ma}}{\partial Fo} + \frac{\dot{m}^*_{ma} Re_f Pr_f}{\rho^{**} A^*_c a^* R_m} \frac{\partial W_{ma}}{\partial z^*} = \frac{Pr_f v^{**}}{Sc_{ma} a^*} \psi \frac{\partial^2 W_{ma}}{\partial z^{*2}} + \frac{Sh_f Pr_f A^*_{fu} v^{**}}{2Sc_{ma} a^*} (W_{sf} - W_{ma}) + \frac{Sh_{wd} Pr_f A^*_{wdu} v^{**}}{Sc_{ma} a^* d^*_{wd}} (W_{swd} - W_{ma}) \quad (37)$$

Initial and boundary conditions

Product and film

$T^*_p = 1.0$ at $Fo \leqslant 0$, for $0 \leqslant r^* \leqslant 1.0$ and $0 \leqslant \theta \leqslant \pi$ (38)

T^*_p remains finite as r^* tends to 0 (39)

$$\lambda^* \left.\frac{\partial T^*_p}{\partial r^*}\right|_{r^*=1} = \left.\frac{\partial T^*_f}{\partial y^*_f}\right|_{y^*_f=0} \text{ and } T^*_p = T^*_f = T^*_{if} \text{ at } r^* = 1.0,$$

for $0 < \theta < \pi$ (40)

$$\frac{\partial T^*_p}{\partial \theta} = 0 \text{ at } Fo > 0, \text{ and at } \theta = 0 \text{ and } \theta = \pi \text{ for } 0 < r^* < 1.0 \quad (41)$$

$$v^*_\theta = 0, \quad \text{at } y^*_f = 0 \quad (42)$$

$$\frac{dv^*_\theta}{dy^*} = 0 \quad \text{at } y^*_f = \delta^* \quad (43)$$

$T^*_f = T^*_{fo}$ at $Fo \leqslant 0$, for $0 \leqslant y^*_f \leqslant \delta^*$ and $0 \leqslant \theta \leqslant \pi$ (44)

$$-\frac{\partial T^*_f}{\partial y^*_f} = B_0 + B_1 T^*_{sf} + B_2 T^{*2}_{sf}$$

at $y^*_f = \delta^*$ and $0 \leqslant \theta \leqslant \pi$, i.e., at the film surface (45)

where B_0, B_1, and B_2 are defined as shown below.

$$B_0 = -\frac{Nu_f \lambda^{**} T^*_{ma}}{2} + \frac{Sh_f Pr_{ma} \lambda^{**}}{2Sc_{ma} C^{**}_p Ja} (C_o - W_{ma})$$

$$B_1 = -\frac{Nu_f \lambda^{**}}{2} + \frac{Sh_f Pr_{ma} \lambda^{**}}{2Sc_{ma} C^{**}_p Ja} C_1 \quad (46)$$

$$B_2 = \frac{Sh_f Pr_{ma} \lambda^{**}}{2Sc_{ma} C^{**}_p Ja} C_2$$

In the above boundary condition, C_0, C_1, and C_2 are the coefficients of a quadratic expression of saturated humidity ratio at the film surface in terms of its temperature and are as follows:

$$W_{sf} = C_0 + C_1 T^*_{sf} + C_2 T^{*2}_{sf} \quad (47)$$

where

$$C_0 = A_0 + A_1 R_T \Delta T + A_2 R^2_T \Delta T^2$$
$$C_1 = A_1 \Delta T + 2A_2 R_T \Delta T^2 \quad (48)$$
$$C_2 = A_2 \Delta T^2$$

$T^*_f = T^*_{fe}$ or T^*_{fbm} for $Fo > 0$, at $\theta = 0$ and $0 < y^*_f < \delta^*$ (49)

The expression for the bulk mean temperature of the film at any angle θ, $T^*_{fbm}|_\theta$, is written as follows:

$$T^*_{fbm} = \left\{ \frac{1}{\dot{m}^*_{ffp}} \int_0^1 2\pi v^*_\theta \sin\theta T^*_f (1 + y^*_f) dy^*_f \right\} \quad (50)$$

$$\frac{\partial T^*_f}{\partial \theta} = 0 \quad \text{at } \theta = \pi \text{ and } 0 \leqslant y^*_f \leqslant \delta^* \quad (51)$$

Water spray

$$\dot{m}^*_{fi} = \dot{m}^*_{fie} = \dot{m}^*_{fe} - \dot{m}^*_{ffe} \quad \text{at } z^* = 0 \quad (52)$$

$$T^*_{wd} = T^*_{fe} \quad \text{at } Fo = 0, \text{ for } 0 \leqslant z^* \leqslant H^* \quad (53)$$

$$T^*_{wd} = T^*_{fe} \quad \text{at } Fo > 0, \text{ and at } z^* = 0 \quad (54)$$

Moist air

$$T^*_{ma} = T^*_{mao} \text{ and } W_{ma} = W_{mao} \quad \text{at } Fo = 0, \text{ for } 0 \leqslant z^* \leqslant H^* \quad (55)$$

$$T^*_{ma} = T^*_{mae} \text{ and } W_{ma} = W_{mae} \quad \text{at } Fo > 0, \text{ and at } z^* = 0 \quad (56)$$

$$\frac{\partial T^*_{ma}}{\partial z^*} = 0 \text{ and } \frac{\partial W_{ma}}{\partial z^*} = 0 \text{ at } z^* = H^* \quad (57)$$

The Nusselt number and the Sherwood number in Equation 46 are evaluated using the following equations (Beukema et al. 1982):

$$Nu_f = 1.27(1 - \psi)^{0.41} Re_p^{0.59} Pr_{ma}^{0.33}$$
$$Sh_f = 1.27(1 - \psi)^{0.41} Re_p^{0.59} Sc_{ma}^{0.33}, \quad \text{for } Re_p > 180 \quad (58)$$

The following correlations are used to determine the Nusselt number and the Sherwood number at the water-droplet surface (Bird et al. 1960).

$$Nu_{wd} = 2.0 + 0.6\, Re^{0.5}_{mwd} Pr^{0.33}_{ma}$$
$$Sh_{wd} = 2.0 + 0.6\, Re^{0.5}_{mwd} Sc^{0.33}_{ma} \quad (59)$$

After finding the air dry-bulb temperature T^*_{ma} and the humidity ratio, W_{ma}, the wet-bulb temperature is determined by solving the following cubic equation:

$$D_1 T^{*3}_{wb} + D_2 T^{*2}_{wb} + D_3 T^*_{wb} = D_4 \quad (60)$$

where

$$D_1 = 2.381C_2\Delta T$$

$$D_2 = 2.381C_1\Delta T + 2.381C_2R_T\Delta T - 2501C_2$$

$$D_3 = 2.381C_0\Delta T + 2.381C_1R_T\Delta T - 2501C_1 - \Delta T - 4.186\Delta T W_{ma}$$

$$D_4 = 2501C_0 - 2.381C_0R_T\Delta T - T^*_{ma}\Delta T - 2501W_{ma} + 2.381R_T\Delta T W_{ma} - 1.805T^*_{ma}\Delta T W_{ma} \quad (61)$$

Method of solution

The following expressions for the film thickness (δ^*) and the tangential velocity (v_θ) are obtained by directly integrating the film momentum equation (Equation 31).

$$\delta^* = \left(\frac{3\mathrm{Fr}_f^2 \dot{m}^*_{ffp}}{2\pi \sin^2\theta\, \mathrm{Re}}\right)^{1/3} \quad (62)$$

$$v^*_\theta = \frac{\mathrm{Re}_f}{\mathrm{Fr}_f^2}\sin\theta\delta^*\left[\frac{y^*_f}{\delta^*} - \frac{1y^{*2}_f}{2\delta^{*2}}\right] \quad (63)$$

The dimensionless governing equations along with the initial and boundary conditions are solved using finite-difference techniques.

In view of the symmetry existing with respect to the vertical axis due to negligible temperature variation in the azimuthal direction, a semicircular region containing the product and the film is considered as the computational domain. The computational domain and the layout of the finite-difference grid are shown in Figure 3. For simplicity, only one product layer with the adjacent air gap is depicted, although a six-layer package is actually considered for analysis. A nonuniform grid is adopted for the solution of moist air and water spray in the interstices between the products. This nonuniform grid is obtained by horizontally extending the radial lines ending on the product surface. In the region between the product layers, a uniform grid is chosen.

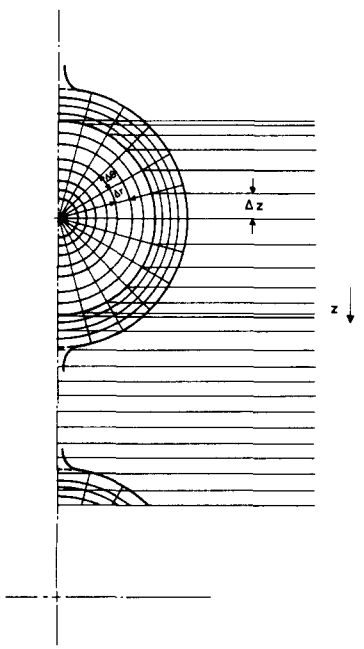

Figure 3 Finite-difference grid system for the product, film, and the accompanying air-spray region

The Peaceman–Rachford Alternating-Direction Implicit (ADI) procedure (Peaceman and Rachford 1955) with forward-time centered-space (FTCS) differencing is employed to simultaneously advance the temperatures in the product and the film from time Fo to time Fo + ΔFo (i.e., from time-level n to $n+1$). The ADI procedure accomplishes this task in two half-time steps. In the first half-time step, the equation is implicit in the r-direction, while in the second half-time step it is implicit in the θ-direction, giving rise, at each half-time step, to a simple tridiagonal system of linear algebraic equations.

The discretized forms of the product and the film energy equations (Equations 30 and 32) for the first half-time step are as follows.

Product

$$(T^{*(n+1/2)}_p - T^{*(n)}_p)/(\Delta\mathrm{Fo}/2) = (T^{*(n+1/2)}_{p,l+1} - 2T^{*(n+1/2)}_{p,l} + T^{*(n+1/2)}_{p,l-1})/(\Delta r^*)^2 + (T^{*(n+1/2)}_{p,l+1} - T^{*(n+1/2)}_{p,l-1})/(r^*_l\Delta r^*) + \cot\theta_m(T^{*(n)}_{p,m+1} - T^{*(n)}_{p,m-1})/(2(r^*_l)^2\Delta\theta) + (T^{*(n)}_{p,m+1} - 2T^{*(n)}_{p,m} + T^{*(n)}_{p,m-1})/(r^*_l\Delta\theta)^2 + q^*_{int} \quad (64)$$

where $r^*_l = (l-1)\Delta r^*$, and $\theta_m = (m-1)\Delta\theta$.

Here the subscripts l and m pertain to r and θ-directions, respectively ($l = 1$ represents the center and $m = 1$ represent the line $\theta = 0$). The default subscripts that are not indicated in the above equation should be taken appropriately. Thus, for instance, $T^{*(n+1/2)}_{p,l+1}$ should actually read $T^{*(n+1/2)}_{p,l+1,m}$.

The above equation can be rearranged to yield the following form:

$$A^p_l T^{*(n+1/2)}_{p,l-1} + B^p_l T^{*(n+1/2)}_{p,l} + C^p_l T^{*(n+1/2)}_{p,l+1} = D^p_l \quad (65)$$

where

$$A^p_l = -1/(\Delta r^*)^2 + 1/(r^*_l\Delta r^*)$$

$$B^p_l = (2/\Delta\mathrm{Fo}) + 2/(\Delta r^*)^2$$

$$C^p_l = -1/(\Delta r^*)^2 - 1/(r^*_l\Delta r^*)$$

$$D^p_l = E^p_m T^{*(n)}_{p,m-1} + F^p_m T^{*(n)}_{p,m} + G^p_m T^{*(n)}_{p,m+1} + q^{*(n)}_{int} \quad (66)$$

where

$$E^p_m = -\cot\theta_m/(2(r^*_l)^2\Delta\theta)) + 1/(r^*_l\Delta\theta)^2$$

$$F^p_m = (2/\Delta\mathrm{Fo}) - 2/(r^*_l\Delta\theta)^2$$

$$G^p_m = \cot\theta_m/(2(r^*_l)^2\Delta\theta) + 1/(r^*_l\Delta\theta)^2 \quad (67)$$

Liquid film

$$(T^{*(n+1/2)}_f - T^{*(n)}_f)/(\Delta\mathrm{Fo}/2) + (\mathrm{Re}_f\,\mathrm{Pr}_f/a^*)v^*_{\theta,l}(T^{*(n)}_{f,m} - T^{*(n)}_{f,m-1})/\Delta\theta = (1/a^*)((T^{*(n)}_{f,m+1} - 2T^{*(n)}_{f,m} + T^{*(n)}_{f,m-1})/(\Delta\theta)^2 + (T^{*(n+1/2)}_{f,l+1} - 2T^{*(n+1/2)}_{f,l} + T^{*(n+1/2)}_{f,l+1})/(\delta^{*(n+1/2)}_m\Delta y^*_f)^2) \quad (68)$$

The above equation can be rearranged to yield the following form:

$$A^f_l T^{*(n+1/2)}_{f,l-1} + B^f_l T^{*(n+1/2)}_{f,l} + C^f_l T^{*(n+1/2)}_{f,l+1} = D^f_l \quad (69)$$

where

$$A^f_l = -1/(a^*(\Delta y^*_f\delta^{*(n+1/2)}_m)^2)$$

$$B^f_l = (2/\Delta\mathrm{Fo}) + 2/(a^*(\Delta y^*_f\delta^{*(n+1/2)}_m)^2)$$

$$C^f_l = A^f_l$$

$$D^f_l = E^f_m T^{*(n)}_{f,m-1} + F^f_m T^{*(n)}_{f,m} + G^f_m T^{*(n)}_{f,m+1} \quad (70)$$

where

$$E_m^f = (\mathrm{Re_f}\,\mathrm{Pr_f} v_\theta^*)/(a^*\Delta\theta) + 1/(a^*(\Delta\theta)^2)$$

$$F_m^f = (2/\Delta\mathrm{Fo}) - (\mathrm{Re_f}\,\mathrm{Pr_f} v_\theta^*)/(a^*\Delta\theta) - 2/(a^*(\Delta\theta)^2)$$

$$G_m^f = 1/(a^*(\Delta\theta)^2) \tag{71}$$

The interface boundary condition (Equation 40) at the product–film interface applicable to the $(n + 1/2)$ time level can be discretized as follows:

$$\lambda^*(T_{\mathrm{p,if}}^{*(n+1/2)} - T_{\mathrm{p,if}-1}^{*(n+1/2)})/\Delta r^* = (T_{\mathrm{f,if}+1}^{*(n+1/2)} - T_{\mathrm{f,if}}^{*(n+1/2)})/(\delta_m^{*(n+1/2)}\Delta y_f^*) \tag{72}$$

The nonlinear boundary condition at the film surface (Equation 45) is linearized and discretized to yield

$$T_{\mathrm{sf}}^{*(n+1/2)} = E_1 + E_2 T_{\mathrm{sf}-1}^{*(n+1/2)} \tag{73}$$

where

$$E_1 = P/Q, \qquad E_2 = 1/Q$$

where

$$P = -\delta_m^{*(n+1/2)}\Delta y_f^*(B_0 - B_2(T_{\mathrm{sf}}^{*(n)})^2)$$

$$Q = 1 + \delta_m^{*(n+1/2)}\Delta y_f^*(B_1 + 2B_2(T_{\mathrm{sf}}^{*(n)})) \tag{74}$$

This linearization is similar to the one employed for radiation boundary conditions (for instance, Carslaw and Jaeger 1955) and is justified in view of the small temperature differences involved. The boundary conditions at $\theta = 0$ and π (Equations 41 and 51) are discretized using two-point one-sided differences.

Equations 65 and 69 when applied to the product and film regions on a radial line along with the interface boundary condition (Equation 72) and the boundary condition at the film surface (Equation 73) and the nth-level center temperature form a set of linear algebraic equations of tridiagonal form, which can be solved using the Thomas algorithm (von Rosenberg, 1969). After sweeping all the radial lines ($m = 2$ to the last but one), the temperatures on the lines $\theta = 0$ and $\theta = \pi$ are calculated. This completes the calculation for the first half-time step.

A similar procedure is used for the second half-time step with the appropriate finite-difference equations.

Owing to the nonexistence of radial symmetry at the center of the food product, the radial gradient cannot be prescribed at the center. Therefore, to calculate the product center temperature, use is made of a local Cartesian mesh, as was employed, for example, by Hwang and Cheng (1970), the applicable equation being

$$\frac{\partial T_{\mathrm{p}}^*}{\partial \mathrm{Fo}} = \frac{\partial^2 T_{\mathrm{p}}^*}{\partial x^{*2}} + \frac{\partial^2 T_{\mathrm{p}}^*}{\partial y^{*2}} + \frac{\partial^2 T_{\mathrm{p}}^*}{\partial z^{*2}} + q_{\mathrm{int}}^* \tag{75}$$

The discretized form of the above equation gives the center temperature in terms of the temperatures at its six nearest neighboring points, four of them (lying in the plane $\theta = \pi/2$) being equal. Thus the center temperature can finally be related to the temperatures of the neighboring points on the lines $\theta = 0$, $\theta = \pi/2$, $\theta = \pi$.

The bulk mean temperature of the film T_{fbm}^*, given by Equation 50, is then calculated using Simpson's rule at the adjacent station to $\theta = \pi$, and this serves as the entry temperature of water to the next product layer. In this manner, the product and film energy equations are solved for all the six layers.

The equation for the water-spray mass conservation (Equation 34) is solved using a simple marching method. The energy equations for the water spray and moist air, as well as the water-vapor conservation equation (Equations 35, 36, and 37), are one-dimensional (1-D) transient equations. The FTCS differencing is adopted for these equations except for the convective terms, for which upwind differences are used (Roache 1982). The discretization of these equations is quite straightforward but lengthy, and therefore is not presented here. These equations are also solved using the tridiagonal matrix algorithm mentioned earlier.

The finite-difference analogues for the second derivatives occurring in the above equations should take into account the nonuniform grid spacing. If F denotes either T_{ma}^* or W_{ma}, and $\Delta z_k^* = \Delta z_{k+1}^* - \Delta z_k^*$, the second derivative F'' with respect to z^* at the grid point k can be written as shown below:

$$F_k'' = 2((\Delta z_k^*/\Delta z_{k-1}^*)F_{k-1} - (1 + \Delta z_k^*/\Delta z_{k-1}^*)F_k + F_{k+1})/(\Delta z_k^*(\Delta z_k^* + \Delta z_{k-1}^*)) \tag{76}$$

The source terms appearing in the discretized equations are evaluated at time-level n wherever necessary.

A number of numerical experiments are performed to determine the grid size and the time step for which the numerical solutions are stable and grid independent. Various grids, with the number of grid points ranging from 13 to 21 in the r-direction (combined product and film region) and from 15 to 23 in the θ-direction, are examined. A grid size of 17 × 19 and a time step of 0.0025 are finally selected as a compromise between the computational time, the memory requirements, and the accuracy. This grid produced temperatures differing in only the fourth decimal place compared to a grid of 21 × 23. The selection of grid size in the product and the film region automatically fixes the number of grid points in the product layer for moist air and the interstitial water spray in the z-direction, as can be visualized from Figure 3. An equal number of uniformly spaced grid points are employed in the accompanying air gaps. All the computations are performed on the computer system VAX 8810. A typical run covering a dimensionless process time of 0.60 took about 250 seconds of CPU time. It may be noted that a dimensionless process time ($\mathrm{Fo} = a_p t/R^2$) of 0.60 corresponds to 48 minutes of physical process time for an average value of $a_p = 1.3 \times 10^{-7}\ \mathrm{m^2 \cdot s^{-1}}$ and for a typical product radius of 0.025 m.

Numerical solutions are obtained for the following values of the parameters so as to cover a wide range of precooling conditions of practical interest.

T_{fe}^* is varied from 0.05 to 0.25. This corresponds to the entering spray water temperature ranging from 4.5 to 11°C.

$\mathrm{Re_f}$ is varied from 5.0 to 50.0 in steps of 5.0. This corresponds to an entering water mass flow rate of 0.017 to 0.17 kg $\mathrm{s^{-1}}$ for the test section having a cross-sectional area of 0.25 $\mathrm{m^2}$.

$\dot{m}_{\mathrm{ma}}^*$ is varied from 1.0 to 10.0 in steps of 1.0. This corresponds to air velocity of 0.17 to 1.7 m $\mathrm{s^{-1}}$ for a film Reynolds number of 30.0.

T_{mae}^* is varied from 0.05 to 0.3438. This corresponds to an entering-air dry-bulb temperature of 4.5°C to 14°C.

W_{mae} is varied from 0.0017 to 0.0046.

λ^* is varied from 0.1 to 1.0 in steps of 0.1. This corresponds to product thermal conductivity of 0.0585 to 0.585 $\mathrm{W \cdot m^{-1} \cdot K^{-1}}$, the thermal conductivity of water being 0.585 $\mathrm{W \cdot m^{-1} \cdot K^{-1}}$. These values cover a wide range of thermal conductivity values for common fruits and vegetables (ASHRAE Handbook of Fundamentals 1989).

ψ is varied from 0.5 to 0.75 in steps of 0.025.

The values of the other parameters are as follows:

$$a^* = 0.9136;\quad a^{**} = 137.5;\quad A_c^* = 400.0;\quad C_p^{**} = 0.2402;$$
$$d_{\mathrm{wd}}^* = 3.4 \times 10^{-2};\quad \mathrm{Fr_f} = 0.003;\quad \mathrm{Ja} = 0.05;\quad L = 6;$$
$$\mathrm{Pr_f} = 7.88;\quad \mathrm{Pr_{ma}} = 0.7482;\quad q_{\mathrm{int}}^* = 0.003;\quad \mathrm{Sc_{ma}} = 0.665;$$
$$\lambda^{**} = 0.042;\quad \rho^{**} = 1.273 \times 10^{-3} \tag{77}$$

It may be noted that the values of A^*_{fu}, A^*_{wdu}, C_0, C_1, C_2, $\dot{m}^*_{ffe}$, $\dot{m}^*_{fie}$, Nu_f, Nu_{wd}, R_m, R_T, Re_p, Re_{mwd}, Sh_f, Sh_{wd}, and v^{**} can be calculated from those of other parameters.

Results and discussion

Typical time–temperature histories are presented in Figure 4. It is observed that the cooling rate is almost the same for all the layers until a certain amount of time. However, after a reasonably long time, the layers reach different steady-state temperatures. It is also found that the bottom layers reach lower temperatures than the top layers. This trend can be explained as follows.

The food products in any layer at any time are cooled by water film enveloping it; the film, in turn, is cooled by the moist air surrounding it. Thus the heat transfer takes place from the products to moist air via the water film. Up to a certain time, these two heat transfer rates balance each other, and hence the food products in all the layers are surrounded by a water film at more or less constant temperature. At larger times, the water film comes in contact with the already cooled product layers, and the simultaneous heat and mass transfer from the water film to the air further reduces the temperature of the film as it flows down the package, resulting in a faster cooling in the bottom layers. For the water over the first layer, the entry temperature is always T^*_{fe}. Evaporative cooling does not seem to manifest itself while the water and air are flowing over the first layer. As a result, the steady-state temperature for the top

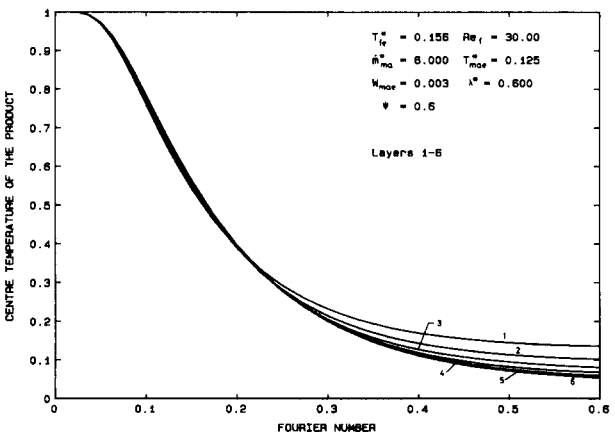

Figure 4 Typical cooling curves during bulk hydraircooling

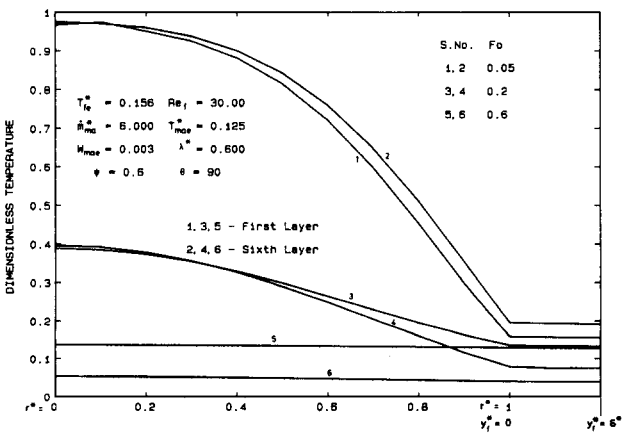

Figure 5 Typical temperature profiles within the product and the film

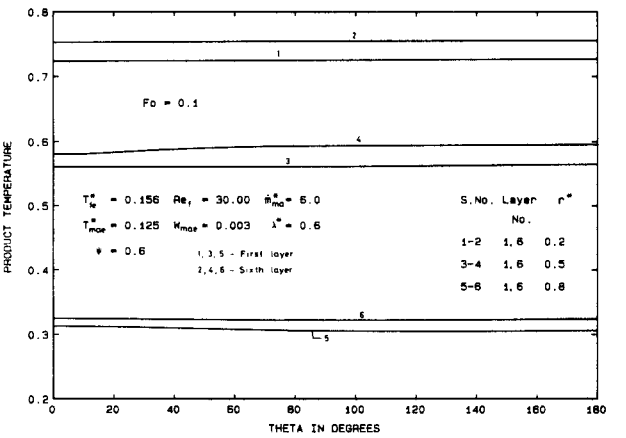

Figure 6 Typical temperature profiles within the product

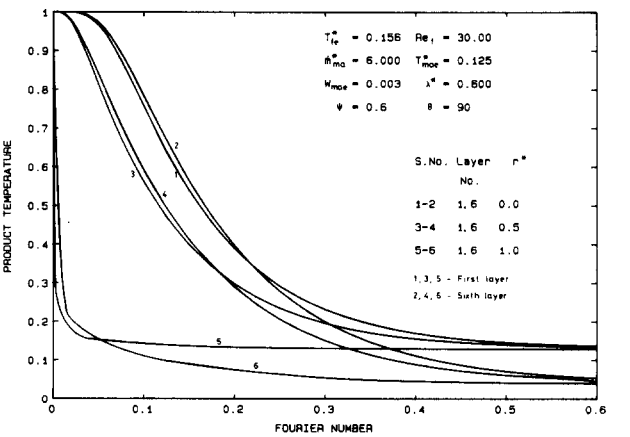

Figure 7 Temperature variation in the radial direction

layer is seen to be limited to the entry water temperature, whereas the bottom layers reach much lower temperatures.

Figure 5 shows typical temperature profiles within the product and the film along the radial line $\theta = \pi/2$ for different times. Temperatures are plotted from the product center to the film outer surface. The film thickness is plotted on a much enlarged scale. It can be seen that the product temperature decreases from the center towards the surface of the product. With increasing time, the temperature profile becomes flatter. It can also be noted that the film temperature variation is insignificant. This may be attributed to the thinness of the film.

The temperature variation in the product in the tangential direction at a time Fo = 0.1 is shown in Figure 6. It can be seen that the product temperature does not vary significantly in the tangential direction.

Figure 7 shows the variation of temperature in the product at a fixed θ and at different radial distances with time Fo. As is expected, the product interior cools more slowly than the surface.

Figure 8 shows the variation of product temperature with time at a fixed radial location and different angular positions. It can be seen that the temperature variation is insignificant with θ.

The numerical results (not shown here) also indicate that the interstitial water mass flow rate decreases by a very small amount as it passes through the package due to negligible evaporation from the water droplets. Figure 9 shows the variation of interstitial water temperature as it passes along the

package. Even a minute quantity of water evaporating from the droplet surface causes a considerable decrease in its temperature because of the large value of the latent heat of evaporation associated with the water. It can be seen that as time progresses, the temperature variation becomes linear.

Figure 10 shows typical variation in the temperature of air, water film, and the interstitial water spray as they pass through the package. The air dry-bulb and wet-bulb temperatures, the film surface temperatures, and the water-droplet temperatures are all plotted on the same graph. It is observed that the air dry-bulb temperature varies almost linearly as it passes through the product layers and is more or less constant between the layers. This is due to the combined effect of (1) the fortuitous property of a sphere by which its surface area varies linearly along any diametral axis and (2) the insignificant angular variation of the water film surface temperature. The moist air exchanges sensible and latent heat both with the film surface and the water droplets. The film has a much larger surface area compared to that of water droplets. In this investigation, the film surface area per unit volume of the package turned out to be about two orders of magnitude higher than the surface area of all the water droplets in the same volume, and hence the individual contribution from the surface of water droplets was negligible. The interstitial water spray passes through the package without much change in its temperature compared to the moist air and the film. It can be seen that the air temperature increases initially but decreases later as it passes through the package. This trend can be explained as follows.

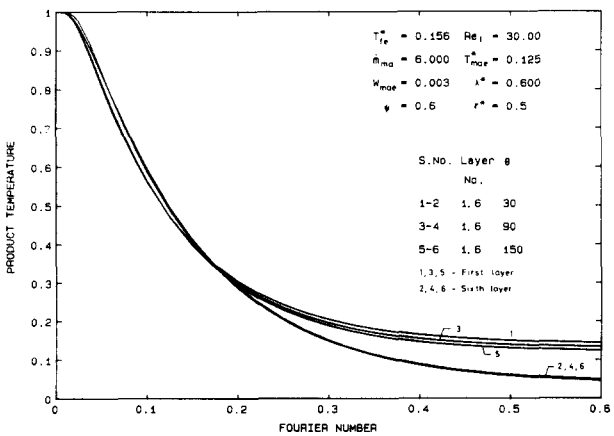

Figure 8 Temperature variation in the tangential direction

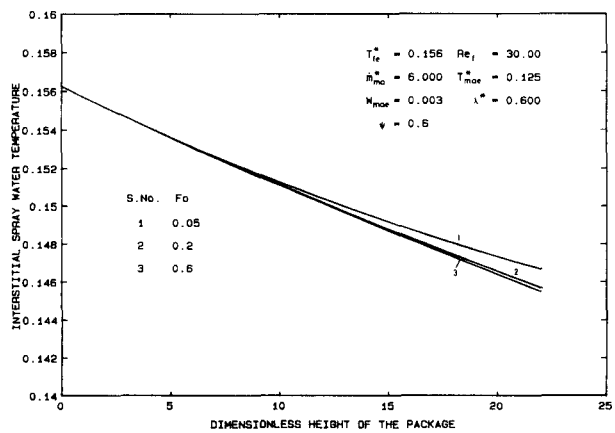

Figure 9 Typical variation of spray water temperature

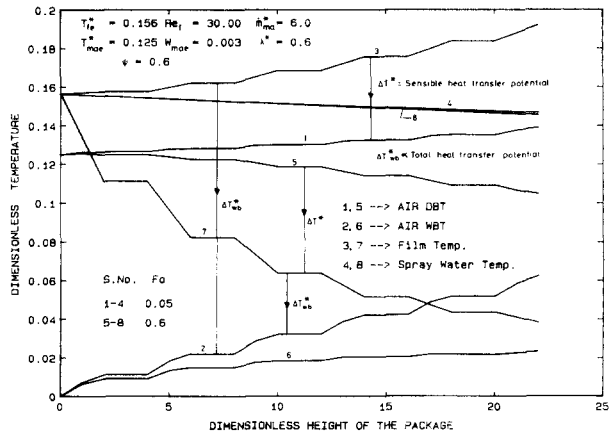

Figure 10 Typical variation of air, spray water, and film temperatures

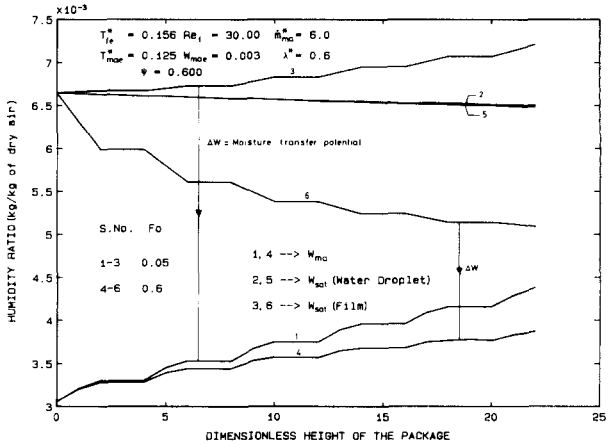

Figure 11 Typical variation of air humidity ratio and the saturated humidity ratio at the water droplet and the film surface

The humid air may receive or lose sensible plus latent heat, depending on the driving potential between air and the film surface at any location. These driving potentials are indicated in Figures 10 and 11. Since the aim of hydraircooling process is to make use of the evaporation from the water film to the air stream as an additional cooling means, the parameters for the water and air such as T_{fe}, T_{mae}, and W_{mae} are so chosen in the present investigation that the air wet-bulb temperature is always lower than that of the water at any location for any time, thus ensuring the transfer of total heat (sensible + latent) from water to air. These parameter values are estimated from a number of numerical experiments. At smaller times, the air picks up heat from the film surface as well as from the surface of water droplets and gets heated up. At larger times, the sensible heat transfer takes place from air to film owing to the lower values of the film temperature, and hence the air gets cooled. Because of the negligible contribution from the surface area of water droplets, the air passes through the air layers without any noticeable change in its temperature. However, since the air wet-bulb temperature is lower than the film temperature at any time and at any location, the total heat transfer takes place from the film and the water droplets to the air.

Figure 11 shows typical variation of the air-humidity ratio W_{ma} and the saturated-humidity ratio at the film and the surface of water droplets. It is observed that the air is becoming more

humid while passing through the package, and the increase in the humidity ratio is more pronounced for the air in the product layers due to the availability of large water film surface area. In the air layers, the air passes without any noticeable change in its humidity ratio. The film surface temperature decreases at larger times, resulting in reduced driving potential for moisture transfer between the film and the air. Hence the moisture transfer with the air gradually decreases with time.

Half cooling time

The half cooling time is based on the entering-air wet-bulb temperature. It is defined as the time required for the initial temperature difference between the product and the entering-air wet-bulb temperature to reduce by one half.

The dimensionless time at which the product center reaches a dimensionless temperature of 0.5 is taken as the half cooling time ($\tau_{1/2}$) and is estimated separately for each of the product layers. From the results of the present analysis, it is observed that the product center temperature reaches a more or less steady value at a process time equal to double the half cooling time with a tolerance of about 5%.

Correlation for half cooling time

A correlating equation for half cooling time in terms of the processing parameters T^*_{fe}, Re_f, $\dot{m}^*_{ma}$, T^*_{mae}, W_{mae}, λ^*, and ψ is developed from the numerical results of the present analysis. The results from 74 computer runs are used for correlating the half cooling time. Because of the different cooling rates exhibited by different layers, correlations are obtained by multiple linear regression analysis for the half cooling time of each layer separately in terms of the governing parameters. The following correlation obtained for the sixth layer is recommended for the entire package, since this layer takes maximum time to reach the half cooling stage.

$$\tau_{1/2} = a0 T^{*a1}_{fe}\, Re^{a2}_f \dot{m}^{*a3}_{ma} T^{*a4}_{mae} W^{a5}_{mae} \lambda^{*a6} \psi^{a7} \qquad (78)$$

where a0, a1, a2, a3, a4, a5, a6, and a7 are regression coefficients and are as shown below:

a0 = 0.3689 a1 = 0.0239 a2 = −0.1126 a3 = −0.107

a4 = 0.0156 a5 = 0.0125 a6 = 0.1154 a7 = 0.0065

Figure 12 shows the practical application of bulk hydraircooling where the time–temperature histories for peaches of 0.05 m diameter are presented. The processing conditions are as follows: product initial temperature, 35°C; spray water temperature, 8°C; mass flow rate of water, 0.1 kg·s^{-1} (the cross-sectional area of the package is taken to be 0.25 m^2); air velocity, 1.0 m s^{-1}; air dry- and wet-bulb temperatures, 6°C and 3°C, respectively, yielding a humidity ratio of 0.0035 kg per kg dry air; void fraction, 0.6.

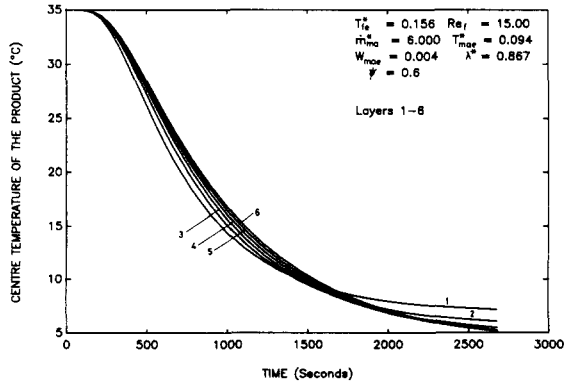

Figure 12 Bulk hydraircooling of peaches

It is seen from the figure that the half cooling time for the sixth layer is about 875 seconds, while the correlation (Equation 78) gives a value of 845 seconds, which compares favorably with the above value.

Comparison with bulk air precooling

Analytical results for the bulk air precooling (simple forced air-cooling of food products in bulk) of spherical food products are reported by Narasaiah Chetty (1987), where the half cooling time for bulk air precooling is correlated as a function of process parameters as shown below.

$$\tau_{1/2} = b0 i^{b1}\, Re^{b2} \psi^{b3} T^{+b4}_{po} u^{b5}_{f0} T^{+b6}_{fowb} \lambda^{b7}_{fp} \qquad (79)$$

where

b0 = 1.1408 b1 = 0.1877 b2 = −0.3991 b3 = −0.1159

b4 = −0.2415 b5 = 0.0113 b6 = 0.0553 b7 = −0.4950

and the parameters are as follows:

i	layer number (layers measured from top to bottom)
Re	air Reynolds number (equivalent to Re_p in the present analysis)
ψ	void fraction (same as in the present analysis)
T^+_{po}	dimensionless product initial temperature ($T^+_{po} = T_{po}/18.83$, T_{po} in degrees Celsius)
u_{fo}	dimensionless air dry-bulb temperature at the entry (equivalent to T^*_{mae} in the present analysis)
T^*_{fowb}	dimensionless air wet-bulb temperature at the entry ($T^+_{fowb} = T_{wbe}/18.83$, T_{wbe} in degrees Celsius)
λ_{fp}	thermal conductivity ratio between the air and the product (equivalent to λ^{**}/λ^* in the present analysis)

In the present investigation, the product initial temperature is assumed to be constant at 35°C, yielding $T^+_{po} = 1.8585$ and for the sixth layer $i = 6$.

This correlation is written in terms of the bulk hydraircooling nomenclature:

$$\tau_{1/2} = c0\, Re^{c1}_p \psi^{c2} T^{*c3}_{mae} T^{c4}_{wbe} \lambda^{*c5} \qquad (80)$$

where

c0 = 7.7544 c1 = −0.3991 c2 = −0.1159 c3 = 0.0113

c4 = −0.0553 c5 = 0.4950

A comparison was made between these two precooling methods in terms of the half cooling time for the sixth layer, and the results are shown in Table 1.

From Table 1 the following observations can be made:

(1) higher spray water temperatures yield higher half cooling times for bulk hydraircooling;
(2) a higher film Reynolds number yields faster cooling for hydraircooling process (cases 6 to 9) (in these cases, the parameter $\dot{m}^*_{ma}$ is also varied such that the air velocity and hence the air Reynolds number remain unchanged);
(3) higher values of air mass flow rate result in faster cooling;
(4) void fractions in the range 0.5 and 0.7 do not have a very significant influence on the results;
(5) larger values of the thermal conductivity ratio yield slower cooling in both the processes;
(6) at higher air-mass flow rates (cases 12 and 13), bulk air precooling enables the products to reach the half cooling stage ahead of bulk hydraircooling.

Table 1 Comparison between the half cooling times of bulk hydraircooling and bulk air precooling calculated from correlations developed from numerical results

Sl. no.	T^*_{fe}	Re_f	$\dot{m}^*_{ma}$	T^*_{mae}	W_{mae}	λ^*	ψ	I	II
1	0.1563	30.0	6.0	0.125	0.0031	0.6	0.6	0.1674	0.1725
2	0.0938	30.0	6.0	0.125	0.0031	0.6	0.6	0.1659	0.1725
3	0.1250	30.0	6.0	0.125	0.0031	0.6	0.6	0.1666	0.1725
4	0.1875	30.0	6.0	0.125	0.0031	0.6	0.6	0.1682	0.1725
5	0.2188	30.0	6.0	0.125	0.0031	0.6	0.6	0.1690	0.1725
6	0.1563	10.0	18.0	0.125	0.0031	0.6	0.6	0.1686	0.1725
7	0.1563	20.0	9.0	0.125	0.0031	0.6	0.6	0.1676	0.1725
8	0.1563	40.0	4.5	0.125	0.0031	0.6	0.6	0.1662	0.1725
9	0.1563	50.0	3.6	0.125	0.0031	0.6	0.6	0.1655	0.1725
10	0.1563	30.0	2.0	0.125	0.0031	0.6	0.6	0.1850	0.2675
11	0.1563	30.0	4.0	0.125	0.0031	0.6	0.6	0.1735	0.2028
12	0.1563	30.0	8.0	0.125	0.0031	0.6	0.6	0.1635	0.1538
13	0.1563	30.0	10.0	0.125	0.0031	0.6	0.6	0.1608	0.1407
14	0.1563	30.0	6.0	0.063	0.0039	0.6	0.6	0.1677	0.1712
15	0.1563	30.0	6.0	0.094	0.0035	0.6	0.6	0.1675	0.1720
16	0.1563	30.0	6.0	0.156	0.0027	0.6	0.6	0.1673	0.1730
17	0.1563	30.0	6.0	0.188	0.0023	0.6	0.6	0.1672	0.1733
18	0.1563	30.0	6.0	0.125	0.0017	0.6	0.6	0.1617	0.1833
19	0.1563	30.0	6.0	0.125	0.0024	0.6	0.6	0.1644	0.1764
20	0.1563	30.0	6.0	0.125	0.0038	0.6	0.6	0.1707	0.1698
21	0.1563	30.0	6.0	0.125	0.0046	0.6	0.6	0.1744	0.1677
22	0.1563	30.0	6.0	0.125	0.0031	0.7	0.6	0.1713	0.1862
23	0.1563	30.0	6.0	0.125	0.0031	0.8	0.6	0.1752	0.1989
24	0.1563	30.0	6.0	0.125	0.0031	0.9	0.6	0.1791	0.2109
25	0.1563	30.0	6.0	0.125	0.0031	1.0	0.6	0.1829	0.2222
26	0.1563	30.0	6.0	0.125	0.0031	0.6	0.5	0.1671	0.1762
27	0.1563	30.0	6.0	0.125	0.0031	0.6	0.55	0.1672	0.1743
28	0.1563	30.0	6.0	0.125	0.0031	0.6	0.65	0.1678	0.1709
29	0.1563	30.0	6.0	0.125	0.0031	0.6	0.7	0.1684	0.1695

Note: I—bulk hydraircooling; II—bulk air precooling.

Conclusions

A mathematical model is developed to describe the simultaneous heat and mass transfer occurring during bulk hydraircooling of spherical food products when the water and air are flowing co-current to each other. The governing equations are solved using finite-difference numerical methods. Some of the important conclusions are as follows:

(1) the products in any layer reach a steady state at a process time that is about double the half cooling time, with a tolerance of about 5%;
(2) the cooling rate of various layers differ by a small amount;
(3) the interstitial water spray does not have any significant effect on the cooling rate;
(4) higher values of film Reynolds number, air-mass flow rate, and lower values of water temperature and thermal conductivity ratio yield faster cooling rates;
(5) bulk air precooling shows a slightly better performance than bulk hydraircooling at higher air-mass flow rates.

References

Abdul Majeed, P. M. (1981) Analysis of heat transfer during hydraircooling of spherical food products. *Int. J. Heat Mass Transfer*, **24**, 323–333

ASHRAE Guide and Data Book (Applications). (1971) American Society of Heating, Refrigerating and Air Conditioning Engineers, Atlanta, GA

ASHRAE Handbook of Fundamentals. (1989) American Society of Heating, Refrigerating and Air Conditioning Engineers, Atlanta, GA

Beukema, K.J., Bruin, S., and Schenk, J. (1982) Heat and mass transfer during cooling and storage of agricultural products. *Chem. Eng. Sci.*, **37**, 291–298

Bird, R. B., Stewart, W. E., and Lightfoot, E. N. (1960) *Transport Phenomena*. John Wiley and Sons, New York

Carslaw, H. S. and Jaeger, J. C. (1959) *Conduction of Heat in Solids*, second ed. Clarendon Press, Oxford

Gaffney, J. J., Baird, C. D., and Chau, K. V. (1985) Methods for calculating heat and mass transfer in fruits and vegetables individually and in bulk. *ASHRAE Trans.*, **91**, Part 2B, 332–352

Hall, E. G. (1974) Techniques of precooling: the long term storage, controlled atmosphere storage and the freezing of fruit and vegetables. *Int. Semin. Application of Refrigeration to Vegetables, Fruits, and Fish in the Forest Region*, C.M.E.R.I., Durgapur, India, D1–D98

Hwang, G. J. and Cheng, K. C. (1970) Boundary vorticity method for convective heat transfer with secondary flow—Application to the combined free and forced laminar convection in horizontal tubes. *Heat Transfer 1970, Proc. Fourth International Heat Transfer Conference*, Paris-Versailles, Vol. IV, Paper No. NC 3.5, Elsevier, Amsterdam, 1970

Krishna Murthy, M. V. and Badarinarayana, K. (1978) Heat and mass transfer in food products. *VI Int. Heat Transfer Conf.*, Toronto, Canada, Aug. 7–11, Vol. 6, 339–353

Narasaiah Chetty, K. (1987) Heat and mass transfer during bulk precooling of food products, Ph.D. Thesis, Indian Institute of Technology, Madras, India

Peaceman, D. W. and Rachford, H. H. (1955) The numerical solution of parabolic and elliptic differential equations. *J. Soc. Indust. App. Math.* **3**, 28–41

Ranz, W. E. and Marshall, W. R. (1952) Evaporation from drops—Part 1. *Chem. Eng. Prog.*, **48**, 141–146

Roache, P. J. (1982) *Computational Fluid Dynamics*. Hermosa, Albuquerque, NM

von Rosenberg, D. U. (1969) *Methods for the Numerical Solution of Partial Differential Equations*. American Elsevier, New York